

# Thermal phase transitions in Artificial Spin-Ice

Demian Levis,<sup>1</sup> Leticia F. Cugliandolo,<sup>1</sup> Laura Foini,<sup>1</sup> and Marco Tarzia<sup>2</sup>

<sup>1</sup>Université Pierre et Marie Curie - Paris 6, Laboratoire de Physique Théorique et Hautes Energies, 4, Place Jussieu, Tour 13, 5ème étage, 75252 Paris Cedex 05, France

<sup>2</sup>Université Pierre et Marie Curie - Paris 6, Laboratoire de Physique Théorique de la Matière Condensée, 4, Place Jussieu, Tour 12, 5ème étage, 75252 Paris Cedex 05, France

We use the sixteen vertex model to describe bi-dimensional artificial spin ice (ASI). We find excellent agreement between vertex densities in fifteen differently grown samples and the predictions of the model. Our results demonstrate that the samples are in usual thermal equilibrium away from a critical point separating a disordered and an anti-ferromagnetic phase in the model. The second-order phase transition that we predict suggests that the spatial arrangement of vertices in near-critical ASI should be studied in more detail in order to verify whether they show the expected space and time long-range correlations.

PACS numbers: 75.50.Lk, 75.10.Hk, 05.70.Jk, 05.70.Ln

Hard local constraints produce a rich variety of collective behavior such as the splitting of phase space into different topological sectors and the existence of “topological phases” that cannot be described with conventional order parameters [1]. In geometrically constrained magnets, the local minimization of the interaction energy on a frustrated unit gives rise to a macroscopic degeneracy of the ground state [2], unconventional phase transitions [3, 4], the emergence of a “Coulomb” phase with long-range correlations [5, 6] and slow dynamics [7, 8] in both 2D and 3D systems. In this work we focus on a paradigm with these features: *spin-ice*, a class of magnets frustrated by the *ice-rules* [9–11].

In *natural spin-ice* the ice rules are due to two facts: the pyrochlore lattice structure, in which rare earth magnetic ions sit on the vertices of corner sharing tetrahedra, and the ferromagnetic interaction between the Ising-like moments that are forced to lie on the edges joining the centers of neighboring tetrahedra by crystal fields. The energy of each unit cell is thus minimized by configurations with two spins pointing in and two out of the center of the cell. All configurations satisfying the local constraint are degenerate ground states if the ice-rule preserving vertices are equally probable. This is the same mechanism whereby water ice has a non-vanishing zero-point entropy that is, indeed, remarkably close to the one of the Dy<sub>2</sub>Ti<sub>2</sub>O<sub>7</sub> spin-ice compound [12]. These materials received a renewed interest in recent years when a formal mapping to magnetostatics suggested to interpret the local configurations violating the spin-ice rule as magnetic charges [13]. However, the detailed study of such defects in 3D remains a hard experimental task.

Bi-dimensional Ising-like ice-models had no experimental counterpart until recently when it became possible to manufacture artificial samples made of arrays of elongated single-domain ferromagnetic nano-islands frustrated by dipolar interactions. The beauty of *artificial spin-ice* (ASI) is that the interaction parameters can be precisely engineered—by tuning the distance between islands, *i.e.* the lattice constant, or by applying external fields—and the microstates can be directly imaged with magnetic force microscopy (MFM) [14]. These systems should set into different phases depending on the ex-

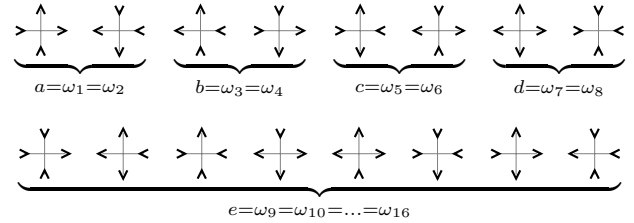


Figure 1. Sixteen vertex configurations and their statistical weights  $\omega_i \propto \exp(-\beta\epsilon_i)$ . The first six-vertices,  $v_1, \dots, v_6$ , verify the ice-rule and have vanishing magnetic charge. Vertices  $v_1, \dots, v_4$  carry a dipolar moment while  $v_5$  and  $v_6$  do not. The last ten vertices are “defects”:  $v_7$  and  $v_8$  have magnetic charge  $\pm 4$  and no dipole moment while  $v_9, \dots, v_{16}$  have magnetic charge  $\pm 2$  and a net dipole moment.

perimental conditions [15]. However, the lack of thermal fluctuations due to the high energy barriers for single spin-flips, had prevented the observation of the expected two-fold degenerate antiferromagnetic (AF) ground state. Recently, these problems have been partially overcome *via* (i) the gradual magneto-fluidization of an initially polarized state [16] and (ii) the thermalization of the system during the slow growth of the samples [17]. Although with de-magnetization the actual AF state of square ASI was never reached, the statistical study of a large number of frozen configurations of samples with up to  $10^6$  vertices at interaction-dominated low energies became possible [16]. With the procedure proposed in (ii) large regions with AF order were formed in a few samples when sufficiently small lattice constant and weak disorder were used. Whether the sampling of a conventional thermal equilibrium ensemble is achieved in this way is a question that was raised in [17, 18] and that we will address here.

The purpose of this letter is to interpret and explain very recent experimental observations on ASI [16–18]. With this aim we consider a simple schematic model for 2D dipolar spin-ice, the *sixteen-vertex model* (see Fig. 1) [4, 8], where dipolar interactions beyond nearest-neighbor vertices are neglected. We compare the equilibrium and out-of-equilibrium properties of the model with the experimental results and we match the behavior of several observables (such as the densities of

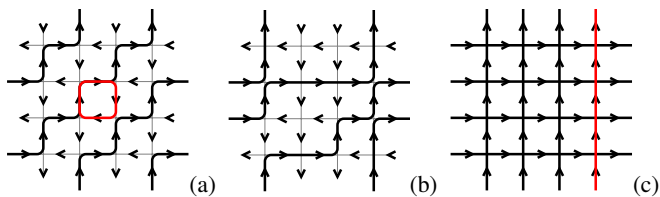


Figure 2. (Color online.) Characteristic configurations of the ground state ( $d = e = 0$ ) of three different phases of the sixteen-vertex model on the square lattice. (a) Antiferromagnetic ( $c$ -AF) order. Reversing the central (red) loop yields an elementary excitation. (b) Collective spin liquid (SL) phase. (c) Frozen ferromagnetic (FM) order. The reversed vertical string (red line) is an extended excitation.

different vertex types  $\langle n_i \rangle$  with data on ASI samples [17, 18]. This approach is at face value similar but actually very different from the one used in previous studies [16, 18], where data were fitted in terms of *single independent vertices* (with no topological interactions), as  $\langle n_i \rangle \propto \exp(-\beta_{\text{eff}} \epsilon_i)$ , with the effective temperature  $\beta_{\text{eff}}$  introduced as a fitting parameter. On the contrary, in our approach frustrated interactions are fully taken into account. This analysis allows us to address the issue of thermalization of ASI samples and to make several predictions that could be tested in the lab.

*The samples and the model.* In their simplest setting ASI are 2D arrays of elongated single-domain permalloy islands whose shape anisotropy defines Ising-like spins arranged along the edges of a regular square lattice. Spins interact through dipolar exchanges and the dominant contributions are the ones between neighboring islands across a given vertex. The sample is frustrated since no configuration of the surrounding spins can minimize all pair-wise dipole-dipole interactions on a vertex. In samples with no height offset ( $h = 0$ ) 2D square symmetry defines four relevant vertex types of increasing energy, where the  $c$  vertices (see Fig. 1) take the lowest value, leading to a ground state with staggered  $c$ -AF order [see Fig. 2(a)]. Note that the relative energies of the different vertex configurations could be tuned by  $h$  in such a way that the ground state displayed FM order [see Fig. 2(c)] [15].

We mimic the experimental samples with the sixteen-vertex model defined as follows: Ising spins sit along the edges of an  $L \times L$  square lattice. Long-range interactions beyond next nearest neighbor spins are neglected and the energies of the sixteen vertex configurations are attributed as explained above. The total energy is given in terms of populations,  $n_i$ , of distinct vertex types,  $E = \sum_{i=1}^{16} n_i \epsilon_i$ , each with a given magnetostatic energy  $\epsilon_i$ . Note that, despite the simple form of  $E$ , nontrivial frustrated topological interactions between vertices *are* present, due to the fact that each pair of neighboring vertices shares the spin sitting along the edge joining them. The model is coupled to a thermal bath at inverse temperature  $\beta$ . We introduce the statistical weights  $\omega_i \propto \exp(-\beta \epsilon_i)$ , that in the literature of vertex models are usually referred as  $a = \omega_1 = \omega_2$ ,  $b = \omega_3 = \omega_4$ ,  $c = \omega_5 = \omega_6$ ,  $d = \omega_7 = \omega_8$  and  $e = \omega_9 = \dots = \omega_{16}$  [4] (see Fig. 1). The equilibrium

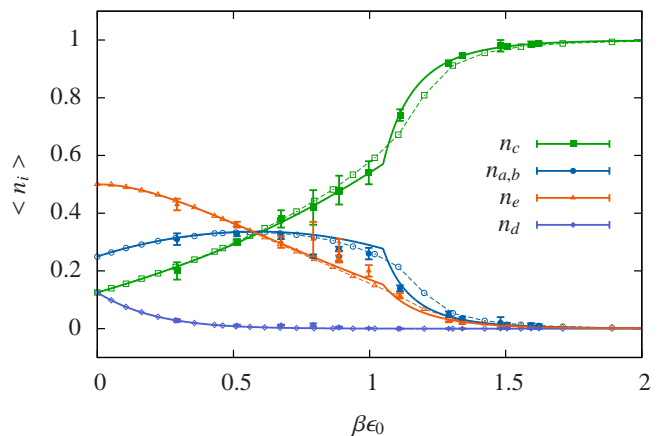


Figure 3. (Color online.) Average densities of different vertex types as a function of  $\beta \epsilon_0$ . Full symbols with error bars are experimental data [18],  $\langle n_i \rangle_{exp}$ . Empty symbols with dotted lines correspond to the equilibrium CTMC data,  $\langle n_i \rangle_{sim}$ . The CVBP analytic solution,  $\langle n_i \rangle_{MF}$ , of the sixteen-vertex model is shown in solid lines.

properties of the model can thus be described in terms of four different statistical weights satisfying  $c > (a = b) > e > d$ .

We study the equilibrium and out-of-equilibrium properties of the sixteen-vertex model in two ways. We perform numerical simulations of the 2D model with a Monte-Carlo algorithm with *single-spin* updates improved with the rejection-free Continuous Time set-up (CTMC). We also employ an analytic approach put forward in [19], based on a sophisticated version of a cluster variational mean-field Bethe-Peierls (CVBP) formalism, by defining the model on a coordination-four tree made of square plaquettes (an extension over the tree of single vertices is necessary to correctly describe an AF phase populated by finite loop fluctuations, see Fig. 2). Details of the calculations have already been extensively reported in [19], where the phase diagram was derived for generic values of the ratios  $a/c$ ,  $b/c$ ,  $d/c$ ,  $e/c$ , showing that the CVBP technique describes with extremely good accuracy the equilibrium properties as compared to MC simulations.

*Density of vertices.* In the experiments in [17, 18] the thickness of the magnetic islands grows by deposition (at constant temperature and all other external parameters within experimental accuracy) on fifteen lattices with five different lattice constants and using three material underlayers (Si, Ti, Cr) in each of them. (We refer to the supplementary material in [18] for more details on the parameters and materials used.) The Ising spins flip by thermal fluctuations during the growth process. However, as the energy barrier for single spin flips increases with the size of the islands, once a certain thickness is reached the barrier crosses over the thermal fluctuations of the bath,  $k_B T$ , and the spins freeze. At the end of the growth process, the spin configurations are imaged with MFM and the number of vertices of each kind are counted on five independent square areas with, roughly,  $27 \times 27$  vertices each. Average values (and statistical errors) are also estimated.

Our analysis is as follows. For each set of vertex concentrations measured in [18] at a given lattice constant, we de-

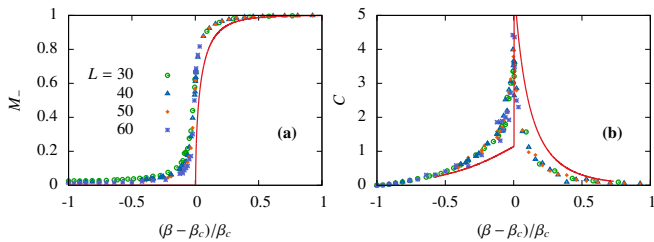


Figure 4. (Color online.) Staggered magnetization  $M_-$  (a) and specific heat  $C$  (b) as a function of the distance to the inverse critical temperature  $\beta_c$  for system sizes  $L = 30, 40, 50, 60$ . The (red) solid lines are the results of the CVBP analytic calculation.

termine the statistical weights  $c$ ,  $a$ ,  $e$ , and  $d$ —and thus  $\beta\epsilon_c$ ,  $\beta\epsilon_a$ ,  $\beta\epsilon_e$ , and  $\beta\epsilon_d$ —that better match the data, by solving the sixteen-vertex model with the CVBP approximation and imposing:

$$\langle n_i \rangle_{exp} = \langle n_i \rangle_{MF} = \frac{\sum_{\mathcal{C}} n_i e^{-\mathcal{H}(a,c,d,e)}}{\sum_{\mathcal{C}} e^{-\mathcal{H}(a,c,d,e)}}, \quad (1)$$

where the sum runs over all possible vertex configurations  $\mathcal{C}$ . Surprisingly enough, it turns out that the energy ratios are approximately constant within the statistical errors for almost all the lattice spacings of the as-grown samples, and coincide with the values used by Nisoli *et al.* [16]. Such energy ratios can be rationalized in term of magnetostatic exchanges due to dipolar interactions between the islands of the sample associated to each vertex configuration. More precisely, each dipole is considered as a pair of oppositely charged monopoles sitting on the vertices, and only Coulomb interactions between monopoles around a single vertex are taken into account, yielding:  $\epsilon_c = 2(1 - 2\sqrt{2})/\ell$ ,  $\epsilon_a = -2/\ell$ ,  $\epsilon_e = 0$ ,  $\epsilon_d = 2(2\sqrt{2} + 1)/\ell$  ( $\ell$  being the lattice constant). As a consequence, the statistical weights of the sixteen-vertex model can be expressed in term of a *single energy scale*  $\epsilon_0$  as  $c = 1$ ,  $a = e^{-\beta\epsilon_0}$ ,  $e = e^{-\beta r_e \epsilon_0}$ , and  $d = e^{-\beta r_d \epsilon_0}$ , with the energy ratios  $r_e$  and  $r_d$  being equal to  $r_e = (2\sqrt{2} - 1)/(2\sqrt{2} - 2) \simeq 2.207$  and  $r_d = 2\sqrt{2}/(\sqrt{2} - 1) \simeq 6.828$ . Remarkably, no fitting parameter nor effective temperature needs to be introduced to describe the data:  $\beta$  is the *true* inverse temperature at which experiments are performed and  $\epsilon_0$  is an energy scale that only depends on the lattice constant and the underlayer, and which could be in principle determined from a microscopic calculation.

In Fig. 3 we plot the thermal averages of the vertex densities as a function of the energy scale  $\beta\epsilon_0$ . The CTMC results ( $\langle n_i \rangle_{sim}$ , empty symbols) and CVBP calculations ( $\langle n_i \rangle_{MF}$ , solid lines) are in excellent agreement. They show a second order phase transition from a paramagnetic (PM) phase at low  $\beta$  to an AF phase dominated by type- $c$  vertices at high  $\beta$ , where both translational invariance and spin reversal symmetry are spontaneously broken. We also include data from [18] (full symbols) that are in remarkable good agreement with the sixteen vertex model curves. (Except for a few points that turn out to be quite close to the critical temperature.)

Such a good agreement confirms that dipolar interactions

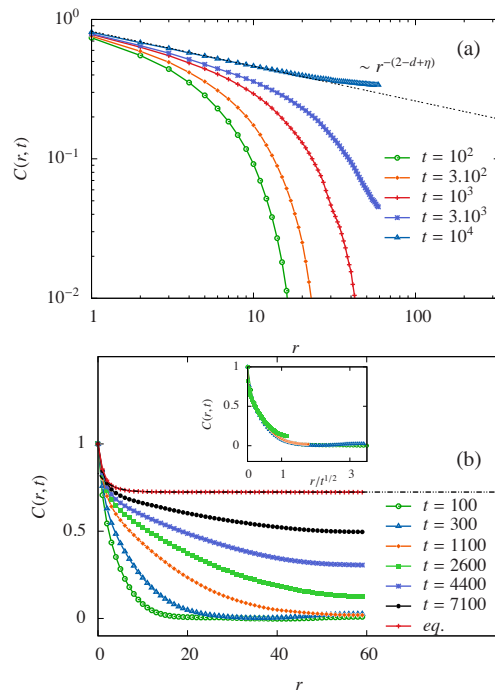


Figure 5. (Color online.) Space-time correlations  $C(r, t)$  after a quench from  $\beta = 0$  to  $\beta_c \approx 1.2$  (a) and  $\beta = 1.36$  (b), in a system with  $L = 60$ . The colored lines-points are data taken at different times. The dotted black lines are the  $t \rightarrow \infty$  equilibrium functions,  $C(r, t \rightarrow \infty) \sim r^{-2+d-\eta}$  with  $\eta = 1/4$ , and  $C(r, t \rightarrow \infty) \sim A \exp(-r/\xi) + M_-^2$ , with  $M_-^2 \approx 0.73$ ,  $\xi \approx 3$ . The inset shows the data in panel (b) where the  $r$ -axis has been rescaled by  $t^{1/2}$ .

beyond nearest neighbor vertices do not play a prominent role and that the sixteen-vertex model mimics ASI samples. It also points out that the simple picture put forward in [16] provides a good estimate of the energy ratios between different vertex types. Finally, and most importantly, these results strongly suggest that the gradual growth of magnetic islands [17, 18] seems to sample the conventional thermal equilibrium ensemble for most of the experimental points.

*Phases and phase transition.* In the following we focus on the PM/AF phase transition. In Fig. 4 we present equilibrium CTMC data for: (a) the order parameter describing  $c$ -AF ordering,  $M_- = \frac{1}{2}(\langle |m_-^x| \rangle + \langle |m_-^y| \rangle)$  where  $m_-^{x,y}$  are the staggered magnetizations along the horizontal and vertical directions; (b) the heat capacity  $C = L^{-2}(\langle E^2 \rangle - \langle E \rangle^2)$  as a function of the distance to the critical inverse temperature,  $(\beta - \beta_c)/\beta_c$ . The data clearly show the presence of a second-order phase transition from a conventional PM phase to a staggered AF phase as  $\beta$  is increased above  $\beta_c \epsilon_0$ . The panels display the analytic results with solid red lines that yield a systematic shift of the critical point by about 10% towards higher temperature, as expected for mean-field calculations. We find  $\beta_c^{MF} = 1.05$  and  $\beta_c^{sim} = 1.2$ , where here and in the following we measure  $\beta$  in units of  $\epsilon_0$ .

We determine  $\beta_c = 1.204 \pm 0.008$  independently with a non-equilibrium relaxation method [20], by identifying  $\beta_c$  as the inverse temperature at which the staggered magnetization

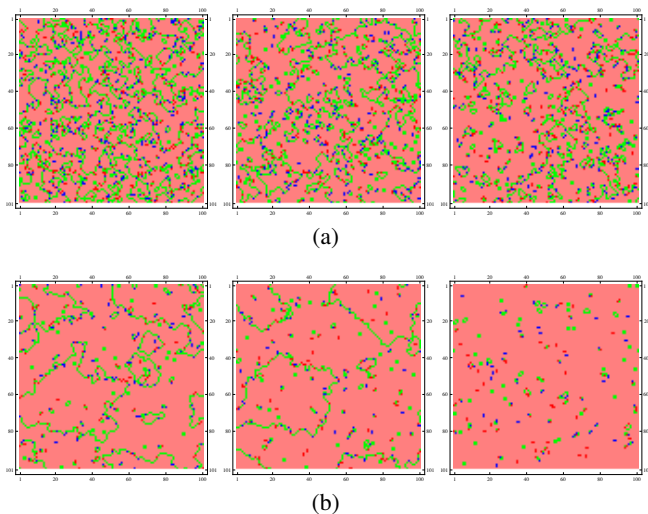


Figure 6. (Color online.) Snapshots of  $L = 10^2$  samples at  $t \simeq 10^2, 10^3, 10^4$  MCs after a quench from  $\beta = 0$  to the critical point,  $\beta_c = 1.2$  (a) and into the AF phase,  $\beta = 1.36$  (b). Pink regions are  $c$ -AF ordered, green points correspond to  $a, b$ -FM vertices, red and blue points correspond to oppositely charged defects of type  $e$ .

has an algebraic decay,  $M_-(t) \sim t^{-\beta/(\nu z_c)}$  as a function of time, where  $\beta$  and  $\nu$  are the equilibrium critical exponents associated to the order parameter and the correlation length, respectively, and  $z_c$  is the dynamical exponent. Away from this temperature an exponential decay is instead observed. This confirms that the criticality of the SL phase [4, 21] is broken by the presence of defects at finite temperature.

**Correlation functions.** Stochastic thermal evolution and canonical equilibration not only yield the vertex densities but also the correlation functions. Figure 5(a) shows the space-dependence of the two-point function  $C(r, t) = L^{-2} \langle \sum_{i,j} S_{i,j}(t) S_{i+r,j+r}(t) \rangle$  at different times after a quench from  $\beta = 0$  to  $\beta_c = 1.2$  (log-log scale).  $S_{i,j}$  denote the spins sitting along the edges of the  $L \times L$  square lattice, with  $S_{i,j} = +1$  if the spin points right or up and  $S_{i,j} = -1$  otherwise.  $r$  is measured in units of  $\ell/\sqrt{2}$ . These data have been averaged over  $10^3$  independent runs of a system with  $L = 60$ . At large times the curves approach the equilibrium asymptotic law characterized by  $C(r, t \rightarrow \infty) \sim r^{-\eta}$  at the critical point, with an exponential cut-off. As shown in the figure (black dotted line), the exponent  $\eta$  remains equal to  $1/4$  in the sixteen-vertex model as it was argued in [19]. This value coincides with the exact result of the eight-vertex [4, 21] and  $2D$  Ising models. Note that the numerical data show clear signs of finite size effects when  $r \approx L$ .

In Fig. 5(b) we show the behavior of  $C(r, t)$  after a quench into the  $c$ -AF phase ( $\beta = 1.36$ ). As shown in [8, 22], the approach to equilibrium is fast if the initial state is a  $T = 0$  ground state whereas it is very slow and occurs *via* a coarsening process if the initial condition is a disordered high temperature one, as for the curves shown in the figure. In equilibrium correlations decay exponentially as  $C(r, t \rightarrow \infty) \sim A \exp(-r/\xi) + M_-^2$  (dotted black line). The asymptotic value  $M_-^2 \approx 0.73$  is consistent with the equilibrium staggered

magnetization shown in Fig. 4, and the correlation length is  $\xi(\beta = 1.36) \approx 3$ . On the other hand, out-of-equilibrium spatial correlations decay to zero at large distances. The data for  $C(r, t)$  at different times shown in Fig. 5(b) collapse onto a single curve when the length variable  $r$  is rescaled by  $t^{1/2}$  (see the inset). This scaling is accurate in a certain time window (i.e. the *coarsening regime*): it fails at times larger than  $\approx 2600$  MCs (as shown in the inset) and smaller than  $\approx 100$  MCs. The snapshots in Fig. 6 and the  $t^{1/2}$  scaling strongly suggests that the system follows a curvature driven type of dynamics during the coarsening regime [23].

These results imply that the samples obtained by using the rotating field protocol [16], where no correlations beyond first-neighbors were observed, have not achieved equilibrium. On the contrary, the as-grown samples in [17, 18] are likely to be near equilibrium. However, as also shown by our numerical results, close to the phase transition critical slowing down sets in, and in the whole AF phase slow coarsening dynamics emerge. It remains therefore to be understood whether critical and subcritical samples have *fully* equilibrated. To settle this issue one should grow samples with a slower deposition rate and measure, if possible, time-dependent observables *during* growth (such as the staggered magnetization and two-times correlation functions). Another possibility is to analyze the spatial correlations. Indeed, the facility of imaging the microstates both numerically and experimentally makes such study very appealing. As an example, in Fig. 6 we show snapshots of microscopic configurations of  $L = 10^2$  systems after quenches from  $\beta = 0$  to  $\beta_c = 1.2$  (a) and  $\beta = 1.36$  (b). The first two panels in each row are out-of-equilibrium while the last ones show typical equilibrium configurations at the critical point and inside the AF phase respectively, cfr. Fig. 5. Large domains of ground state AF order form, separated by domain walls made by  $a$  and  $b$  vertices. The size of the AF domains increases with time as equilibrium is approached. These snapshots could be compared with MFM images of ASI configurations of [17, 18] at the corresponding values of  $\beta$  (the experimental points closest to  $\beta_c = 1.2$  and  $\beta = 1.36$  correspond to the samples produced using a Ti underlayer with lattice constants  $\ell = 466$  nm and  $\ell = 433$  nm, respectively).

**Conclusion.** In this letter we studied the equilibrium and out-of-equilibrium properties of the  $2D$  sixteen-vertex model using MC simulations and a sophisticated cluster variational Bethe-Peierls approach, and we compared our results to the recent experimental data on ASI [16–18]. We showed that the model describes with very good accuracy the behavior of the densities of the different vertex types of the ASI samples obtained by gradual deposition of magnetic material on a square pattern as the lattice constant and the underlayer disorder are changed, resulting in a change of the statistical weights of the different vertex types. This implies that the experimental samples of [17, 18] are at—or at least very close to—thermal equilibrium. It is important to point out that our interpretation does not require any fitting parameter as the effective temperature introduced in [16, 18]. We reveal the presence of a second order phase transition from a conventional high tem-

perature (large lattice constant, strong disorder) PM phase to a low temperature (small lattice constant, weak disorder) staggered AF phase. Such a phase transition could have a major impact on thermalization and full equilibration, and could be unveiled by measuring long-range spatial correlations in the experiments.

We close by insisting upon the fact that, although vertex models avoid all the complications of (long-range) dipolar interactions, they provide a very good schematic framework to study ASI from a theoretic perspective. The excitement around these samples as well as the intriguing excitation properties of spin-ice (emergence of magnetic monopoles and attached Dirac strings [13]) should encourage their study from a novel and more phenomenological perspective.

*Acknowledgments:* We thank T. Blanchard, C. Castellano, C. Nisoli for very useful discussion and G. Brunell, J. Morgan and C. Morrows for lending their experimental data to us. We acknowledge financial support from ANR-BLAN-0346 (FAMOUS).

- 
- [2] R. Moessner and A. P. Ramirez, *Phys. Today* **59**, 24 (2006).
  - [3] L. D. C. Jaubert *et al.*, *Phys. Rev. Lett.* **100**, 1 (2008).
  - [4] E. H. Lieb and F. Y. Wu, in *Phase transitions and critical phenomena Vol. 1*, edited by C. Domb and J. L. Lebowitz (Academic Press, 1972), chap. 8, p. 331.
  - [5] R. Youngblood *et al.*, *Phys. Rev. B* **21**, 5212 (1980).
  - [6] C. Henley, *Ann. Rev. Cond. Matt. Phys.* **1**, 179 (2010).
  - [7] T. Fennell *et al.*, *Phys. Rev. B* **72**, 1 (2005).
  - [8] D. Levis and L. F. Cugliandolo, *EPL* **97**, 30002 (2012).
  - [9] M. J. Harris *et al.*, *Phys. Rev. Lett.* **79**, 2554 (1997).
  - [10] S. T. Bramwell and M. J. Gingras, *Science* **294**, 1495 (2001).
  - [11] S. T. Bramwell *et al.*, in *Frustrated spin systems*, edited by H. T. Diep (World Scientific, 2004), chap. 7.
  - [12] A. Ramirez *et al.*, *Nature* **399**, 333 (1999).
  - [13] C. Castellano *et al.*, *Nature* **451**, 42 (2008).
  - [14] R. F. Wang *et al.*, *Nature* **439**, 303 (2006).
  - [15] G. Möller and R. Moessner, *Phys. Rev. Lett.* **96**, 1 (2006).
  - [16] C. Nisoli *et al.*, *Phys. Rev. Lett.* **105**, 1 (2010).
  - [17] J. P. Morgan *et al.*, *Nature Phys.* **7**, 75 (2010).
  - [18] J. P. Morgan *et al.*, *Phys. Rev. B* **87**, 024405 (2013).
  - [19] L. Foini *et al.*, *J. Stat. Mech.* p. P02026 (2013).
  - [20] E. V. Albano *et al.*, *Rep. Prog. Phys.* **74**, 026501 (2011).
  - [21] R. J. Baxter, *Exactly solved models in statistical mechanics*, vol. 9 (Dover, 1982).
  - [22] Z. Budrikis *et al.*, *J. App. Phys.* **111**, 07E109 (2012).
  - [23] A. J. Bray, *Advances in Physics* **43**, 357 (1994).

[1] L. Balents, *Nature* **464**, 199 (2010), ISSN 1476-4687.